Scientific Research Publishing

Journal of Applied Mathematics and Physics, 2025, 13(1), 281-301
https://www.scirp.org/journal/jamp
ISSN Online: 2327-4379
ISSN Print: 2327-4352

A Simulated Unified Resultant Amplitude Method for Multi-Dimensional/Multi-Variable Opposite Wave Summation

Shawn P. Guillory

Department of Mechanical Engineering, The University of Louisiana at Lafayette, Lafayette, USA
Email: shawn.guillory1@louisiana.edu

How to cite this paper: Guillory, S.P. (2025) A Simulated Unified Resultant Amplitude Method for Multi-Dimensional/Multi-Variable Opposite Wave Summation. *Journal of Applied Mathematics and Physics*, **13**, 281-301.
https://doi.org/10.4236/jamp.2025.131013

Received: December 3, 2024
Accepted: January 23, 2025
Published: January 26, 2025

Abstract

The simulated unified resultant amplitude theory studies function and polar graphs of sinusoidal radial waves including the cosine, sine, and summation waves for determining separate combination-wave equations arising from 2D spatial oscillator fields in each of the four quadrants corresponding to the *x*-*y* Cartesian reference frame. Combination-wave fluctuations in terms of their algebraic signs are then extrapolated and mathematically modeled relative to the quadrant number by way of Euler's equation. The resulting sign fluctuation equations are used to synthesize the combination-wave equations into a single unified equation along with a unified wave rotation solution that adequately represents all four quadrant-specific wave equations. Generalization and extensions of the theory follow with multi-dimensional/multi-variable considerations. Subsequently, utilization of the theory regarding an applied mathematics and physics-based kinematics motion problem, a generalized differential equation solution for a spring system, as well as a four-dimensional/four-variable dual-cone example are provided for validating the methodology. Consequently, it is shown that the proposed unified model is useful for performing a compact resultant amplitude analysis within general applications involving various wave phenomena.

Keywords

Waves, Resultant Amplitude, Euler's Equation, Unified Theory, Spectral Analysis, Kinematics

1. Introduction

Within the development of mathematical theories applicable to a wide variety of engineering problems, there are many cases where opposite wave summation

equations are prevalent to the specific task being solved. Several examples include time and frequency domain analysis encountered with vibrating systems involving rectilinear and torsional springs, gravitational arrangements, centrifugal machines, and more which are comprised of simple harmonic equations as demonstrated by the phasor model in the first quadrant of the rectangular Cartesian plane [1] [2]. Moreover, there are several other related engineering applications such as those regarding the study of harmonic oscillators, the plotting of spectral energies involving musical instruments in connection with the Fourier series, and spectral wave analysis for modeling water ripples [3]-[6]. Other related applications involve signal analysis for analyzing AC electrical circuits, the application of partial differential equations for heat transfer in thermal systems, and several considerations for vorticity arising in circular and helical fluid flow problems among others [7] [8].

Expanding on subjects regarding vorticity, due to an interesting connection between combination waves and the nature of fluid elements rotating in the vicinity of vortex flow, the discussion provided by Liu *et al.* on flow deflection characteristics for incompressible fluids in the vortex chamber extrapolated from an analysis of its influencing parameters having an inclusion of combination waves are explored [8] [9]. Other sources of vorticity extending beyond the flow of fluids may arise in the study of various electron orbital shapes in the quantum mechanical model due to energy level fluctuations and atomic hybridization [10]. Conversely, and on a cosmological level, the magnetic fields of the Earth's polar axis are represented by polar wave fields comprised of combination waves producing a vortex-like space field [11]. In relation to this space field, Houston and Dymnikov present a spherically symmetric solution of the metric matrix equation for the symmetrical matrix field in the four-dimensional metric space which provides indication of vorticity due to its spherical nature [12]. To further mention, Haramein describes the nature of a vortex space within a presentation associated with the formulation of torque and Coriolis force terms in Einstein's field equations for describing the origin of spin [13].

With this in mind, and within a review of various kinds of analyses focused more toward four-quadrant combination wave productions, an illustration of the photorefractive crystal arising from two interacting beams within the works of Engin, Cross, and Yariv involve four-wave mixing due to the propagation of two-dimensional vector fields of light waves in each of the four quadrants of the Cartesian plane [14]. In relation, the *k*-space configuration for four-wave mixing mimics polar plots of radial summation waves occupying two consecutive quadrants.

For further theoretical exploration, Cuyt and Lee discuss parametric spectral analysis involving multiscale matrix pencils for separable reconstruction problems which explore scaling and shifting of sine and cosine waves [15]. Additionally, Webb et al. describe Alfven simple waves for Euler potentials and magnetic helicity involving summation wave characteristics [16]. Moreover, Islam, Kumar,

and Akbar present a unified method applied to the new Hamiltonian amplitude equation including summation waves nested within four clusters for considering disabilities of modulation wave-train equations [17].

Moving further, and with considerations regarding higher order mathematical matters, the concept of infinitary logic within John T. Baldwin's study of complex numbers and complex exponentiation including a mix of 38 examples, definitions, theorems, corollaries, assumptions, lemmas, and notation math sentence structures having o-minimal and quasiminimal characteristics is presented [18]. Other related mathematics include Köplinger's and Shuster's exceptional infinite fields with distributive exponentiation as well as the works of Prots'ko and Gryshchuk for software development implementation involving the computation of modular exponentiation with precomputation of a reduced set of residues on universal computer systems [19] [20].

However, and despite such expansiveness regarding the detailed and complex theory presented within related areas of mathematics, existing literature is lacking a directly usable unified approach to collectively analyzing resultant amplitude problems in relation to the specific type and application presented in this research for purposes of generalizing related applications of the theory. Therefore, we develop a unified combination-wave equation for unifying summation waves pertaining to the four different quadrants of the Cartesian reference frame through implementation of Euler's parametric complex exponentiation equation. In connection, we also provide a wave rotation solution of the unified wave equation for unifying the eight different solutions that arise from the four distinct wave summations. The proposed methodology is comprised of the following steps: (1) deriving separate combination-wave equations for symbolic unification of their corresponding component waves; (2) unifying the combination-wave equations into one expression for all waves; (3) solving for the wave rotation angle from the unified wave equation; (4) generalizing and extending the theory to multi-dimensional/multi-variable considerations; and (5) numerical validation involving application of the unified wave rotation solution to a 2D physics-based kinematics motion problem, a generalized differential equation solution for a spring system, as well as a four-dimensional/four-variable dual-cone example.

2. Methodology

2.1. Derivation of Separate Combination-Wave Equations

In this resultant amplitude theory, we consider radial cosine waves having amplitude a, radial sine waves having amplitude b, and radial summation waves in polar form to examine plane waves that describe spatial oscillators about a point source.

$$r_A(\theta) = a\cos\theta \tag{1}$$

$$r_B(\theta) = b\sin\theta \tag{2}$$

$$r_C(\theta) = a\cos\theta + b\sin\theta \tag{3}$$

The function and polar graphs for these waves are presented in Figure 1 to aid in understanding the following derivation regarding combination-wave equations.

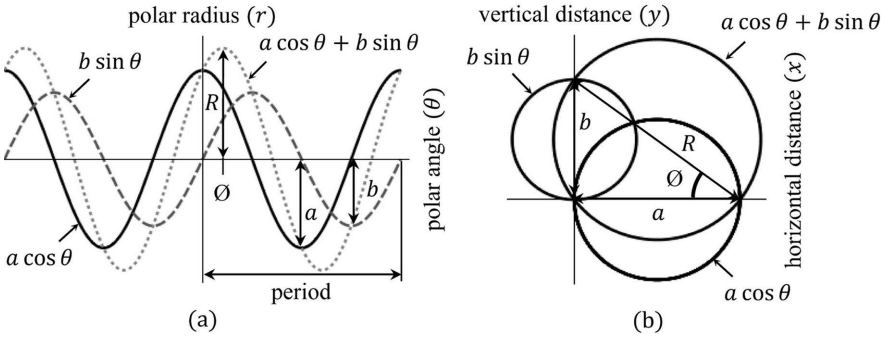

Figure 1. (a) Radial plane wave function graph, (b) Radial plane wave polar graph.

The summation wave, shown in Figure 1(a) and Figure 1(b), represents a right-shifted/tilted radial cosine wave (due to the phase angle $\varnothing$) with a resultant amplitude/diameter R as defined by Equations (4) and (5).

$$R = \sqrt{a^2 + b^2} \tag{4}$$

$$\varnothing = \tan^{-1}\left|\frac{b}{a}\right| \tag{5}$$

The triangle formation from the polar plot within Figure 1(b), as shown in Figure 2 below, indicates that the maximum wave radii are aligned along cosine and sine amplitude axes [2]. This property shows that the radial cosine, sine, and summation waves are illustrated within the first quadrant of the Cartesian plane. Their behavior is then extended to all four quadrants, and the algebraic sign fluctuations in the cosine and sine wave components are extrapolated to form the basis for a simulated unified combination-wave model.

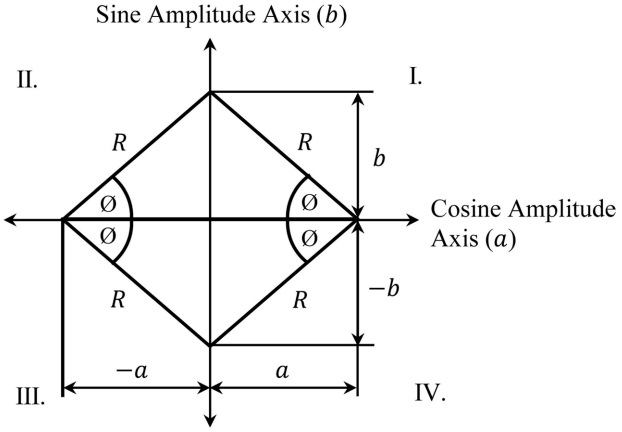

Figure 2. Triangle Formations within the polar plane wave fields.

The waves in each quadrant, shown in Figure 3(a) and Figure 3(b), are described by separate Equations (6) to (9) which are then transformed into a more

condensed form (called combination-waves) using amplitude normalization and sum-to-product identities.

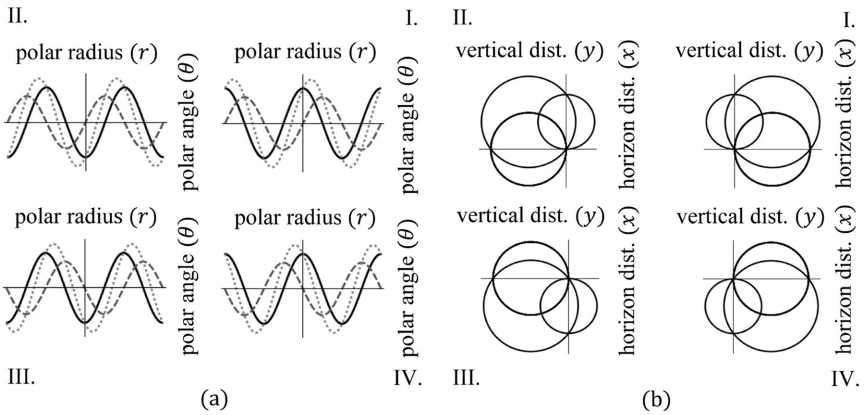

Figure 3. (a) Four radial wave function graphs, (b) Four radial wave polar graphs.

$$r_{C1}(\theta) = a\cos\theta + b\sin\theta = R\cos(\theta - \varnothing) \tag{6}$$

$$r_{C2}(\theta) = -a\cos\theta + b\sin\theta = -R\cos(\theta + \varnothing) \tag{7}$$

$$r_{C3}(\theta) = -a\cos\theta - b\sin\theta = -R\cos(\theta - \varnothing) \tag{8}$$

$$r_{C4}(\theta) = a\cos\theta - b\sin\theta = R\cos(\theta + \varnothing) \tag{9}$$

Table 1. Combination-wave algebraic sign fluctuations.

Combination Waves	Resultant Amplitude Sign Fluctuations	Phase Angle Sign Fluctuations
$R\cos(\theta - \varnothing)$	+1	−1
$-R\cos(\theta + \varnothing)$	−1	+1
$-R\cos(\theta - \varnothing)$	−1	−1
$R\cos(\theta + \varnothing)$	+1	+1

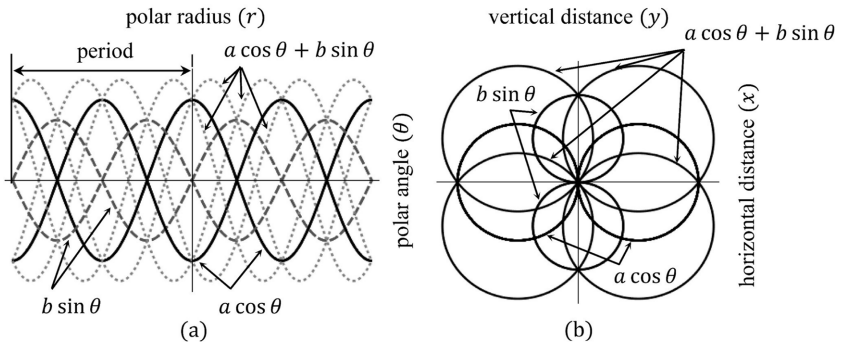

Figure 4. (a) Unified radial wave function graph, (b) Unified radial wave polar graph.

The four combination-wave equations for each quadrant are similar but differ in the algebraic signs of their resultant amplitudes and phase angles. Table 1

illustrates these differences, and the unification process involves combining these wave models into one expression that connects them through all four quadrants as represented by Figure 4(a) and Figure 4(b) above.

2.2. Unification of the Separate Combination-Wave Equations

To restate, the primary distinction between each quadrant's summation wave equation lies in the signs of resultant amplitudes and phase angles. The unified combination-wave model is grounded in Euler's Equation (10), which connects the quadrants through bounded rotational motion in the complex plane, as depicted in Figure 5 below.

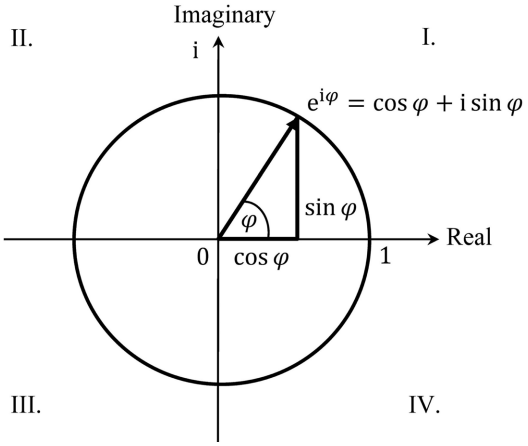

Figure 5. Euler's complex number equation.

$$e^{i\varphi} = \cos\varphi + i\sin\varphi \tag{10}$$

Unification is achieved by using Euler's identity, provided with Equation (11) showing Euler's equation at $\varphi = n\pi$, to relate the wave fluctuations across quadrants, ensuring that the combination-wave fluctuations $\hat{R}$ and $\hat{\varnothing}$ can be described using a *single* unified equation.

$$e^{in\pi} = \operatorname{cis} n\pi = \begin{cases} +1 & n = 0 \vee \text{even} \\ -1 & n = \text{odd} \end{cases} \tag{11}$$

Table 2 demonstrates the relation between the quadrant number/spatial property q versus the alternate positive and negative quantities of unity arising from Euler's identity.

Table 2. Euler's identity versus the quadrant number/spatial property.

q	n	Euler's Identity (where $n = q - 1$)		
1	0	$\cos 0\pi + i\sin 0\pi \Rightarrow$	$+1 + 0i \Rightarrow$	$+1$
2	1	$\cos 1\pi + i\sin 1\pi \Rightarrow$	$-1 + 0i \Rightarrow$	-1
3	2	$\cos 2\pi + i\sin 2\pi \Rightarrow$	$+1 + 0i \Rightarrow$	$+1$
4	3	$\cos 3\pi + i\sin 3\pi \Rightarrow$	$-1 + 0i \Rightarrow$	-1

The algebraic sign changes in Euler's identity, as shown in Table 2, leads to the conclusion that successive multiplication and the negative of these quantities each provide exact mathematical correlations to the sign fluctuations in the resultant amplitude and phase angle as previously shown in Table 1. Table 3 provides an outline of these calculations with respect to the quadrant number.

Table 3. Mathematical determination of $\hat{R}$ and $\hat{\varnothing}$.

q	n	Values for R Sign Fluctuations	Values for $\varnothing$ Sign Fluctuations
1	0	$e^{i(0)} = +1$	$-e^{i(0)} = -1$
2	1	$e^{i(0)}e^{i(\pi)} = -1$	$-e^{i(\pi)} = +1$
3	2	$e^{i(0)}e^{i(\pi)}e^{i(2\pi)} = -1$	$-e^{i(2\pi)} = -1$
4	3	$e^{i(0)}e^{i(\pi)}e^{i(2\pi)}e^{i(3\pi)} = +1$	$-e^{i(3\pi)} = +1$

Due to the pattern shown in Table 3, we use the N-Ary product operator $\prod f(n)$ to represent the successive multiplication procedure for $\hat{R}$ which is then expanded with the Floor function. We also show the mathematical relations for $\hat{R}$ and $\hat{\varnothing}$ in terms of the absolute value operator thereby eliminating the need for prescribing a quadrant number.

$$\hat{R} = \prod_{m=1}^{q} e^{i(m-1)\pi} \Rightarrow (-1)^{\text{Floor}\left(\frac{q}{2}\right)} \equiv \frac{a}{|a|} \quad q = 1,2,3,4 \tag{12}$$

$$\hat{\varnothing} = -e^{i(q-1)\pi} \Rightarrow -\cos\pi(q-1) - i\sin\pi(q-1) \equiv -\frac{ab}{|ab|} \quad q = 1,2,3,4 \tag{13}$$

Since we have a mathematical model for determining the algebraic sign fluctuations, we can effectively write the *four* separate combination-wave equations as one unified equation and show its conversion into summation wave form thereby illustrating the cosine and sine wave components.

$$r_{Cq}(\theta) = \hat{R}R\cos\left(\theta + \hat{\varnothing}\varnothing\right) = \hat{R}|a|\cos\theta - \hat{R}\hat{\varnothing}|b|\sin\theta \tag{14}$$

This unification is validated by resolving the unified summation and combination-wave models into their separate wave equations, through evaluations of $\hat{R}$ and $\hat{\varnothing}$ relative to the quadrant number, which confirms that the unified equation can represent all quadrant-specific behaviors. Three validation methods are provided for the unified wave equation in summation and combination-wave forms: evaluation based on the N-Ary product, Floor function, and absolute value operators.

For the summation wave, we have:

$$\begin{aligned} r_{C1}(\theta) &= \left(\prod_{m=1}^{q=1} e^{i(m-1)\pi}\right) a\cos\theta - \left(\prod_{m=1}^{q=1} e^{i(m-1)\pi}\right)\left(-e^{i(1-1)\pi}\right) b\sin\theta \\ &\Rightarrow a\cos\theta + b\sin\theta \\ &\equiv (-1)^{\text{Floor}\left(\frac{1}{2}\right)} a\cos\theta + (-1)^{\text{Floor}\left(\frac{1}{2}\right)}\left(-e^{i(1-1)\pi}\right) b\sin\theta \end{aligned} \tag{15}$$

$$\Rightarrow a\cos\theta + b\sin\theta$$

$$\equiv \frac{+a}{|+a|}a\cos\theta + \frac{+a}{|+a|}\frac{(+a)(+b)}{|(+a)(+b)|}b\sin\theta \Rightarrow a\cos\theta + b\sin\theta$$

$$r_{C2}(\theta) = \left(\prod_{m=1}^{q=2} \mathrm{e}^{\mathrm{i}(m-1)\pi}\right) a\cos\theta - \left(\prod_{m=1}^{q=2} \mathrm{e}^{\mathrm{i}(m-1)\pi}\right)\left(-\mathrm{e}^{\mathrm{i}(2-1)\pi}\right) b\sin\theta$$

$$\Rightarrow -a\cos\theta + b\sin\theta \tag{16}$$

$$\equiv (-1)^{\mathrm{Floor}\left(\frac{2}{2}\right)} a\cos\theta + (-1)^{\mathrm{Floor}\left(\frac{2}{2}\right)}\left(-\mathrm{e}^{\mathrm{i}(2-1)\pi}\right) b\sin\theta$$

$$\Rightarrow -a\cos\theta + b\sin\theta$$

$$\equiv \frac{-a}{|-a|}a\cos\theta + \frac{-a}{|-a|}\frac{(-a)(+b)}{|(-a)(+b)|}b\sin\theta \Rightarrow -a\cos\theta + b\sin\theta$$

$$r_{C3}(\theta) = \left(\prod_{m=1}^{q=3} \mathrm{e}^{\mathrm{i}(m-1)\pi}\right) a\cos\theta - \left(\prod_{m=1}^{q=3} \mathrm{e}^{\mathrm{i}(m-1)\pi}\right)\left(-\mathrm{e}^{\mathrm{i}(3-1)\pi}\right) b\sin\theta$$

$$\Rightarrow -a\cos\theta - b\sin\theta \tag{17}$$

$$\equiv (-1)^{\mathrm{Floor}\left(\frac{3}{2}\right)} a\cos\theta + (-1)^{\mathrm{Floor}\left(\frac{3}{2}\right)}\left(-\mathrm{e}^{\mathrm{i}(3-1)\pi}\right) b\sin\theta$$

$$\Rightarrow -a\cos\theta - b\sin\theta$$

$$\equiv \frac{-a}{|-a|}a\cos\theta + \frac{-a}{|-a|}\frac{(-a)(-b)}{|(-a)(-b)|}b\sin\theta \Rightarrow -a\cos\theta - b\sin\theta$$

$$r_{C4}(\theta) = \left(\prod_{m=1}^{q=4} \mathrm{e}^{\mathrm{i}(m-1)\pi}\right) a\cos\theta - \left(\prod_{m=1}^{q=4} \mathrm{e}^{\mathrm{i}(m-1)\pi}\right)\left(-\mathrm{e}^{\mathrm{i}(4-1)\pi}\right) b\sin\theta$$

$$\Rightarrow a\cos\theta - b\sin\theta \tag{18}$$

$$\equiv (-1)^{\mathrm{Floor}\left(\frac{4}{2}\right)} a\cos\theta + (-1)^{\mathrm{Floor}\left(\frac{4}{2}\right)}\left(-\mathrm{e}^{\mathrm{i}(4-1)\pi}\right) b\sin\theta$$

$$\Rightarrow a\cos\theta - b\sin\theta$$

$$\equiv \frac{+a}{|+a|}a\cos\theta + \frac{+a}{|+a|}\frac{(+a)(-b)}{|(+a)(-b)|}b\sin\theta \Rightarrow a\cos\theta - b\sin\theta$$

For the combination wave, we have:

$$r_{C1}(\theta) = \left(\prod_{m=1}^{q=1} \mathrm{e}^{\mathrm{i}(m-1)\pi}\right) R\cos\left(\theta + \left(-\mathrm{e}^{\mathrm{i}(1-1)\pi}\right)\varnothing\right) \Rightarrow R\cos(\theta - \varnothing) \tag{19}$$

$$\equiv (-1)^{\mathrm{Floor}\left(\frac{1}{2}\right)} R\cos\left(\theta - \mathrm{e}^{\mathrm{i}(1-1)\pi}\varnothing\right) \Rightarrow R\cos(\theta - \varnothing)$$

$$\equiv \frac{+a}{|+a|} R\cos\left(\theta - \frac{(+a)(+b)}{|(+a)(+b)|}\varnothing\right) \Rightarrow R\cos(\theta - \varnothing)$$

$$r_{C2}(\theta) = \left(\prod_{m=1}^{q=2} \mathrm{e}^{\mathrm{i}(m-1)\pi}\right) R\cos\left(\theta + \left(-\mathrm{e}^{\mathrm{i}(2-1)\pi}\right)\varnothing\right) \Rightarrow -R\cos(\theta + \varnothing) \tag{20}$$

$$\equiv (-1)^{\mathrm{Floor}\left(\frac{2}{2}\right)} R\cos\left(\theta - \mathrm{e}^{\mathrm{i}(2-1)\pi}\varnothing\right) \Rightarrow -R\cos(\theta + \varnothing)$$

$$\equiv \frac{-a}{|-a|} R\cos\left(\theta - \frac{(-a)(+b)}{|(-a)(+b)|}\varnothing\right) \Rightarrow -R\cos(\theta+\varnothing)$$

$$r_{C3}(\theta) = \left(\prod_{m=1}^{q=3} \mathrm{e}^{\mathrm{i}(m-1)\pi}\right) R\cos\left(\theta + \left(-\mathrm{e}^{\mathrm{i}(3-1)\pi}\right)\varnothing\right) \Rightarrow -R\cos(\theta-\varnothing) \tag{21}$$

$$\equiv (-1)^{\mathrm{Floor}\left(\frac{3}{2}\right)} R\cos\left(\theta - \mathrm{e}^{\mathrm{i}(3-1)\pi}\varnothing\right) \Rightarrow -R\cos(\theta-\varnothing)$$

$$\equiv \frac{-a}{|-a|} R\cos\left(\theta - \frac{(-a)(-b)}{|(-a)(-b)|}\varnothing\right) \Rightarrow -R\cos(\theta-\varnothing)$$

$$r_{C4}(\theta) = \left(\prod_{m=1}^{q=4} \mathrm{e}^{\mathrm{i}(m-1)\pi}\right) R\cos\left(\theta + \left(-\mathrm{e}^{\mathrm{i}(4-1)\pi}\right)\varnothing\right) \Rightarrow R\cos(\theta+\varnothing) \tag{22}$$

$$\equiv (-1)^{\mathrm{Floor}\left(\frac{4}{2}\right)} R\cos\left(\theta - \mathrm{e}^{\mathrm{i}(4-1)\pi}\varnothing\right) \Rightarrow R\cos(\theta+\varnothing)$$

$$\equiv \frac{+a}{|+a|} R\cos\left(\theta - \frac{(+a)(-b)}{|(+a)(-b)|}\varnothing\right) \Rightarrow R\cos(\theta+\varnothing)$$

2.3. Isolation of the Polar Angle/Combination-Wave Rotation

In some cases, isolating the polar angle/combination-wave rotation θ is useful, particularly when r_{Cq} is a known quantity c_q regarding a specific application. The unified combination-wave equation allows for its solution to be derived in a compact manner without needing to isolate the angle for each of the four combination-wave equations separately.

Rearranging the combination-wave Equation (14), with the incorporation of clockwise and counterclockwise angle domain assumptions as well as an inclusion of reference angles and their coterminal angles represented as $m\pi$, we have:

$$\cos\left(\pm\left(\theta + \hat{\varnothing}\varnothing + m\pi\right)\right) = \frac{c_q}{\hat{R}R} \qquad m = 0, \pm1, \pm2, \pm3, \cdots, \pm\infty. \tag{23}$$

Finally, we isolate the combination-wave rotation solution as follows.

$$\theta = \pm\cos^{-1}\frac{c_q}{\hat{R}R} - \hat{\varnothing}\varnothing - m\pi \tag{24}$$

Consequently, a general unified clockwise/counterclockwise combination-wave rotation solution is provided by Equation (24).

2.4. Generalization and Extensions to Multiple Dimensions/Variables

To extend this simulated unified resultant amplitude theory toward a generalized consideration of multi-dimensional/multi-variable problems, we assign the cosine and sine wave amplitudes each with their own sets of infinitely many independent dimensions/variables. This accounts for the possibility of the cosine amplitude varying in certain dimensions/variables, such as time and magnetic fields, while the sine amplitude varies in other dimensions/variables, such as temperature and electric fields. In connection, the unified summation/combination wave Equation

(25) below contains the polar angle variable in conjunction with the cosine and sine wave amplitudes' independent dimension variables. The polar angle may also be considered as a function having its own set of dimensions which would replace the polar angle variable with its dimensions inside the function notation for the dependent variable.

Furthermore, and while this theory relied on the study of 2D spatial oscillators, the equality between the summation wave and its combination-wave form along with its corresponding wave rotation solution remain valid for any type of wave behavior, e.g., the 3D spatial sinusoidal wave behavior of electromagnetism arising from AC phenomena. To make a proper distinction of this, the dependent variable g_{cq} is used to represent any quantity (such as a rectangular coordinate distance, the moment of a force versus time, the Hamiltonian of a system, etc.) rather than using the radial variable r_{cq}.

$$\begin{aligned} & g_{cq}\left(\theta, N_{A1}, N_{B1}, \cdots, N_{An}, N_{Bn}\right) \\ & = \hat{R}\left|a\left(N_{A1}, N_{A2}, \cdots, N_{An}\right)\right|\cos\theta - \hat{R}\hat{\varnothing}\left|b\left(N_{A1}, N_{A2}, \cdots, N_{An}\right)\right|\sin\theta \\ & = \hat{R}R\left(N_{A1}, N_{B1}, \cdots, N_{An}, N_{Bn}\right)\cos\left(\theta + \hat{\varnothing}\varnothing\left(N_{A1}, N_{B1}, \cdots, N_{An}, N_{Bn}\right)\right) \end{aligned} \tag{25}$$

When independent variables in the cosine and/or sine amplitudes include the polar angle, it is important to note that the combination-wave rotation solution provided is not applicable and cannot be generalized over the many equation classes that can arise with an inclusion of this angle. Nevertheless, a generalized wave rotation solution of Equation (25) is provided below due to its assumption of having amplitudes that are free of the polar angle.

$$\begin{aligned} & \theta\left(N_{\theta 1}, N_{\theta 2}, \cdots, N_{\theta n}\right) = \theta\left(N_{A1}, N_{B1}, \cdots, N_{An}, N_{Bn}\right) \\ & = \pm\cos^{-1}\frac{c_q\left(N_{A1}, N_{B1}, \cdots, N_{An}, N_{Bn}\right)}{\hat{R}R\left(N_{A1}, N_{B1}, \cdots, N_{An}, N_{Bn}\right)} - \hat{\varnothing}\varnothing\left(N_{A1}, N_{B1}, \cdots, N_{An}, N_{Bn}\right) - m\pi \end{aligned} \tag{26}$$

Regarding amplitudes varying by the polar angle, we make note that the unified combination-wave equation can be generalized to consider summations of opposite waves having different frequencies as well as horizontal and vertical shifts. To account for this, the following equation provides a more general summation wave equation where the independent polar angle is replaced with its possible dimensions and where f is frequency, h is the horizontal shift, and v is the vertical shift. Moreover, this summation wave can be expressed as a combination-wave when using the amplitude Equations (27) and (28).

$$a\left(\theta, N_{A1}, N_{A2}, \cdots, N_{An}\right) = A\left(\theta, N_{A1}, N_{A2}, \cdots, N_{An}\right)\frac{\cos\left(f_a\theta + h_a\right)}{\cos\theta} \tag{27}$$

$$b\left(\theta, N_{A1}, N_{A2}, \cdots, N_{An}\right) = B\left(\theta, N_{A1}, N_{A2}, \cdots, N_{An}\right)\frac{\sin\left(f_b\theta + h_b\right)}{\sin\theta} \tag{28}$$

$$\begin{aligned} & g_{cq}\left(\theta, N_{A1}, N_{B1}, \cdots, N_{An}, N_{Bn}\right) \\ & = \hat{R}\left|A\left(\theta, N_{A1}, N_{A2}, \cdots, N_{An}\right)\right|\cos\left(f_a\theta + h_a\right) \\ & \quad - \hat{R}\hat{\varnothing}\left|B\left(\theta, N_{A1}, N_{A2}, \cdots, N_{An}\right)\right|\sin\left(f_b\theta + h_b\right) + \left(v_a + v_b\right) \end{aligned}$$

$$= \hat{R}R\left(\theta, N_{A1}, N_{B1}, \cdots, N_{An}, N_{Bn}\right)\cos\left(\theta + \hat{\varnothing}\varnothing\left(\theta, N_{A1}, N_{B1}, \cdots, N_{An}, N_{Bn}\right)\right) + \left(v_a + v_b\right) \tag{29}$$

3. Results with Results Discussion

3.1. 2D Physics-Based Kinematics Wave Equation Application

The following validation method for the unified resultant amplitude theory involves the unified combination-wave equation and its wave rotation solution. This method is applied within a two-dimensional physics-based kinematics motion example of an arm that rotates counterclockwise due to a motor as shown in Figure 6 below. The rotating arm varies in only one variable, specifically by variable θ, the indefinite polar angle.

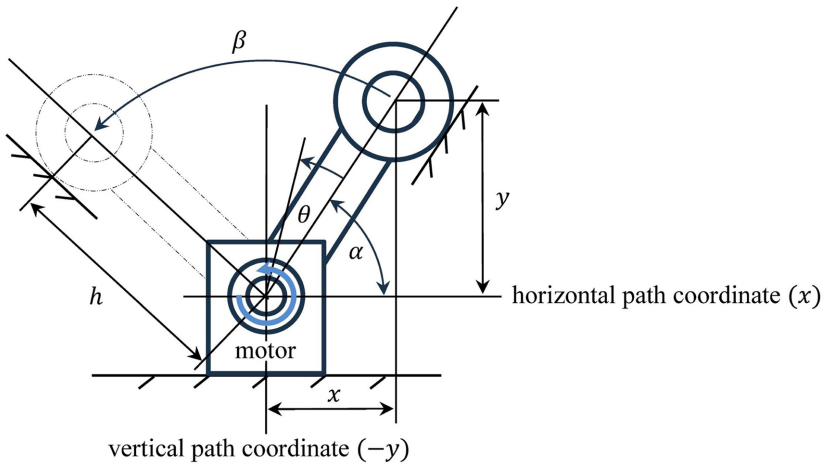

Figure 6. Kinematic layout of a rotating arm mechanism.

The kinematics example is modeled by prescribing values for the initial rotational arm path coordinates as $x_o = 2$ meters and $y_o = 3$ meters, which serve as the absolute values of URAM amplitudes a and b respectively. The resultant amplitude and phase angles follow from this convention.

$$R = \sqrt{x_o^2 + y_0^2} = h \tag{30}$$

$$\varnothing_x = \tan^{-1}\left|\frac{y_o}{x_o}\right| = \alpha \tag{31}$$

$$\varnothing_y = \tan^{-1}\left|\frac{x_o}{y_o}\right| = \frac{\pi}{2} - \alpha \tag{32}$$

The well-known transformation equation approach specific to the rotational arm path indicates that:

$$x\left(\theta\right) = h\cos\left(\alpha + \theta\right) \Rightarrow x_o\cos\theta - y_o\sin\theta, \tag{33}$$

$$y\left(\theta\right) = h\sin\left(\alpha + \theta\right) \Rightarrow x_o\sin\theta + y_o\cos\theta. \tag{34}$$

As seen within Equations (33) and (34), they consecutively contain amplitudes

$a_x = x_o$ and $b_x = -y_o$ in conjunction with $a_y = x_o$ and $b_y = y_o$. Therefore, and with the quadrant numbers being four for $x(\theta)$ and one for $y(\theta)$, the combination-wave equations for the parametric path equations are:

$$x(\theta) = \prod_{m=1}^{4} e^{i(m-1)\pi} R\cos\left(\theta - e^{i(1-1)\pi}\varnothing_x\right) \Rightarrow R\cos\left(\theta + \varnothing_x\right), \tag{35}$$

$$y(\theta) = \prod_{m=1}^{1} e^{i(m-1)\pi} R\cos\left(\theta - e^{i(1-1)\pi}\varnothing_y\right) \Rightarrow R\cos\left(\theta - \varnothing_y\right). \tag{36}$$

Consequently, the wave rotation solution for this specific problem is:

$$\theta = \pm\cos^{-1}\frac{c_x}{R} - \varnothing_x - m_x\pi = \pm\cos^{-1}\frac{c_y}{R} + \varnothing_y - m_y\pi. \tag{37}$$

To note, the summation wave numbers, c_x and c_y, are chosen to each be Equations (33) and (34) respectively with substitution of chosen polar angle values.

Table 4. Kinematics validation of combination-wave equations and wave rotation solution.

Polar Angle	Typical Path Method		URAM Path Method		Percent Errors		+Spin Angle Choice		−Spin Angle Choice		Percent Errors-1		Percent Errors-2	
θ	$x(\theta)$	$y(\theta)$	$x(\theta)$	$y(\theta)$	E_x	E_y	θ_{x1}	θ_{y1}	θ_{x2}	θ_{y2}	$E_{\theta x1}$	$E_{\theta y1}$	$E_{\theta x2}$	$E_{\theta y2}$
0˚	2.00	3.00	2.00	3.00	0.00	0.00	0.0	67.4	−112.6	0.0	0.00	N/A	N/A	0.00
20˚	0.85	3.50	0.85	3.50	0.00	0.00	20.0	47.4	−132.6	20.0	0.00	N/A	N/A	0.00
40˚	−0.40	3.58	−0.40	3.58	0.00	0.00	40.0	40.0	−152.6	387.4	0.00	0.00	N/A	N/A
60˚	−1.60	3.23	−1.60	3.23	0.00	0.00	60.0	60.0	−172.6	7.4	0.00	0.00	N/A	N/A
80˚	−2.61	2.49	−2.61	2.49	0.00	0.00	80.0	80.0	−192.6	−12.6	0.00	0.00	N/A	N/A
100˚	−3.30	1.45	−3.30	1.45	0.00	0.00	100.0	100.0	−212.6	−32.6	0.00	0.00	N/A	N/A
120˚	−3.60	0.23	−3.60	0.23	0.00	0.00	120.0	120.0	−232.6	−52.6	0.00	0.00	N/A	N/A
140˚	−3.46	−1.01	−3.46	−1.01	0.00	0.00	107.4	140.0	140.0	−72.6	N/A	0.00	0.00	N/A
160˚	−2.91	−2.14	−2.91	−2.14	0.00	0.00	87.4	160.0	160.0	−92.6	N/A	0.00	0.00	N/A
180˚	−2.00	−3.00	−2.00	−3.00	0.00	0.00	67.4	180.0	180.0	−112.6	N/A	0.00	0.00	N/A
200˚	−0.85	−3.50	−0.85	−3.50	0.00	0.00	47.4	200.0	200.0	−132.6	N/A	0.00	0.00	N/A
220˚	0.40	−3.58	0.40	−3.58	0.00	0.00	27.4	207.4	220.0	220.0	N/A	N/A	0.00	0.00
240˚	1.60	−3.23	1.60	−3.23	0.00	0.00	7.4	187.4	240.0	240.0	N/A	N/A	0.00	0.00
260˚	2.61	−2.49	2.61	−2.49	0.00	0.00	−12.6	167.4	260.0	260.0	N/A	N/A	0.00	0.00
280˚	3.30	−1.45	3.30	−1.45	0.00	0.00	−32.6	147.4	280.0	280.0	N/A	N/A	0.00	0.00
300˚	3.60	−0.23	3.60	−0.23	0.00	0.00	−52.6	127.4	300.0	300.0	N/A	N/A	0.00	0.00
320˚	3.46	1.01	3.46	1.01	0.00	0.00	320.0	107.4	−72.6	320.0	0.00	N/A	N/A	0.00
340˚	2.91	2.14	2.91	2.14	0.00	0.00	340.0	87.4	−92.6	340.0	0.00	N/A	N/A	0.00
360˚	2.00	3.00	2.00	3.00	0.00	0.00	360.0	67.4	−112.6	360.0	0.00	N/A	N/A	0.00

Polar radii for the angle solutions are chosen to be the path coordinates found from the typical path method. The table entries colored blue and gray represent the angle solutions using c_x and c_y respectively. The entries containing angle values that required an addition of -2π are colored in a darker color shade than the others.

As shown within Table 4 above, wave Equations (35) and (36) are numerically compared with wave Equations (33) and (34). Subsequently, wave rotation solution values deriving from Equation (37) are compared with the chosen polar angle values to demonstrate the validity of the results and theory specific to the first and fourth quadrants thereby validating the theory.

While all angle values shown in the table satisfy the unified combination-wave equation, the results demonstrate that the angle values in the colored entries adequately represent the kinematics example problem. Additionally, the angle solution changes between clockwise and counterclockwise arccosine solution types for every one-half of a revolution made by the rotating arm starting from the positive horizontal axis.

Further validation regarding the second and third quadrants are provided within the following example application of a generalized differential equation solution for a spring system.

3.2. The Generalized ODE Displacement Solution for 2D Spring Systems

A general solution to the inhomogeneous ordinary differential Equation (38) models four spring system types due to the included external properties of free and forced vibrations in conjunction with undamped and damped material behaviors.

$$m_o\ddot{x}(t)+c\dot{x}(t)+kx(t)=f(t) \quad x_o=x(t_o), v_o=\dot{x}(t_o) \tag{38}$$

Within this equation, the specified fixed variables include the mass m_o attached to the end of a spring, the tendency constant c for the spring to produce damped motion, and the stiffness k of the spring. The functions $x(t)$ and $f(t)$ are denoted as the temporal-domain spring displacement equation and the external force application respectively. The associated differential equation solution utilizes initial conditions rather than boundary conditions in alignment with the typical practices of vibration analysis.

Furthermore, various vibration characteristics regarding natural angular frequency, critical damping, the damping ratio, and damped angular frequency are defined in accordance with the following equations.

$$\omega_n=\sqrt{\frac{k}{m_o}} \tag{39}$$

$$c_c=2m_o\omega_n \tag{40}$$

$$\zeta=\frac{c}{c_c} \tag{41}$$

$$\omega_d=\sqrt{1-\zeta^2}\omega_n \tag{42}$$

Related constants of integration $\mathbb{C}_1$ and $\mathbb{C}_2$ pertaining to the spring displacement equation are provided where the non-integral and integral terms correspond to complementary and particular solution components of the full differential

equation solution.

$$\mathbb{C}_1 = \mathbb{C}_{c1} + \mathbb{C}_{p1} = \mathrm{e}^{\zeta\omega_n t_o}\left(x_o\cos\left(\omega_d t_o\right) - \left(\frac{v_o + \zeta\omega_n x_o}{\omega_d}\right)\sin\left(\omega_d t_o\right)\right) + \frac{1}{m_o\omega_d}\int_0^{t_o}\mathrm{e}^{\zeta\omega_n t} f\left(t\right)\sin\left(\omega_d t\right)\mathrm{d}t \tag{43}$$

$$\mathbb{C}_2 = \mathbb{C}_{c2} + \mathbb{C}_{p2} = \mathrm{e}^{\zeta\omega_n t_o}\left(x_o\sin\left(\omega_d t_o\right) + \left(\frac{v_o + \zeta\omega_n x_o}{\omega_d}\right)\cos\left(\omega_d t_o\right)\right) - \frac{1}{m_o\omega_d}\int_0^{t_o}\mathrm{e}^{\zeta\omega_n t} f\left(t\right)\cos\left(\omega_d t\right)\mathrm{d}t \tag{44}$$

The full generalized differential equation solution for spring displacement is:

$$\begin{aligned} x\left(t\right) &= x_c\left(t\right) + x_p\left(t\right) \\ &= \mathrm{e}^{-\zeta\omega_n t}\left(\mathbb{C}_1 - \frac{1}{m_o\omega_d}\int \mathrm{e}^{\zeta\omega_n t} f\left(t\right)\sin\left(\omega_d t\right)\mathrm{d}t\right)\cos\left(\omega_d t\right) \\ &\quad + \mathrm{e}^{-\zeta\omega_n t}\left(\mathbb{C}_2 + \frac{1}{m_o\omega_d}\int \mathrm{e}^{\zeta\omega_n t} f\left(t\right)\cos\left(\omega_d t\right)\mathrm{d}t\right)\sin(\omega_d t) \end{aligned} \tag{45}$$

where the non-integral terms represent the homogenous aspect, and the integral terms arise from inhomogeneity.

Table 5. Dual-cone validation of combination-wave equations and wave rotation solution.

Time	Typical ODE Method		URAM ODE Method		Percent Errors		Angle	+Spin Angle Choice		−Spin Angle Choice		Percent Errors-1		Percent Errors-2	
t	$x_2(t)$	$x_3(t)$	$x_2(t)$	$x_3(t)$	E_{x2}	E_{x3}	$\omega_d t$	$\theta_{q2,1}$	$\theta_{q3,1}$	$\theta_{q2,2}$	$\theta_{q3,2}$	$E_{\theta q2,1}$	$E_{\theta q3,1}$	$E_{\theta q2,2}$	$E_{\theta q3,2}$
0	−0.87	−0.61	−0.87	−0.61	0.00	0.00	0.0	0.0	125.5	−107.1	0.0	0.00	N/A	N/A	0.00
0.25	0.20	−1.17	0.20	−1.17	0.00	0.00	45.0	45.0	80.2	−152.2	45.0	0.00	N/A	N/A	0.00
0.5	1.00	−1.00	1.00	−1.00	0.00	0.00	90.1	90.1	90.1	−196.8	34.2	0.00	0.00	N/A	N/A
0.75	1.14	−0.30	1.14	−0.30	0.00	0.00	135.1	119.7	135.1	135.1	−11.8	N/A	0.00	0.00	N/A
1	0.65	0.47	0.65	0.47	0.00	0.00	180.2	76.7	180.2	180.2	−56.6	N/A	0.00	0.00	N/A
1.25	−0.10	0.88	−0.10	0.88	0.00	0.00	225.2	32.5	225.2	225.2	−98.9	N/A	0.00	0.00	N/A
1.5	−0.66	0.77	−0.66	0.77	0.00	0.00	270.3	−14.9	220.6	270.3	270.3	N/A	0.00	0.00	N/A
1.75	−0.74	0.28	−0.74	0.28	0.00	0.00	315.3	315.3	179.7	−65.9	315.3	0.00	0.00	N/A	N/A
2	−0.38	−0.25	−0.38	−0.25	0.00	0.00	360.4	360.4	134.5	−117.0	360.4	0.00	0.00	N/A	N/A

Polar radii for the angle solutions are chosen to be the path coordinates found from the typical ODE method. The table entries that are colored blue and gray apply to the specific example problem. The entries containing angle values that required an addition of -2π are colored in a darker color shade than the others.

Within Table 5 above, using $m_o = 3$ kg, $c = 2$ kg/s, $k = 30$ N/m, and $f\left(t\right) = t$ N, validation of this URAM theory involves the numerical evaluation of Equations (50) and (51) which model the unified combination-wave representation of the spring's displacement along with its wave rotation solution. Moreover, the numerical validation uses $x_o = 1$ m, $v_o = 2$ m/s, and $t_o = 0.5$ s to create

waves in the second quadrant in addition to using $x_o = -1$ m, $v_o = 2$ m/s, and $t_o = 0.5$ s for creating waves in the third quadrant.

$$a(t) = \mathrm{e}^{-\zeta\omega_n t}\left(\mathbb{C}_1 - \frac{1}{m_o\omega_d}\int \mathrm{e}^{\zeta\omega_n t} f(t)\sin(\omega_d t)\,\mathrm{d}t\right) \tag{46}$$

$$b(t) = \mathrm{e}^{-\zeta\omega_n t}\left(\mathbb{C}_2 + \frac{1}{m_o\omega_d}\int \mathrm{e}^{\zeta\omega_n t} f(t)\cos(\omega_d t)\,\mathrm{d}t\right) \tag{47}$$

$$R(t) = \sqrt{a^2(t) + b^2(t)} \tag{48}$$

$$\varnothing(t) = \tan^{-1}\left|\frac{b(t)}{a(t)}\right| \tag{49}$$

$$x(t) = \frac{a(t)}{|a(t)|}R(t)\cos\left(\omega_d t + \frac{a(t)b(t)}{|a(t)b(t)|}\varnothing(t)\right) \tag{50}$$

$$\theta(t) = \omega_d t = \pm\cos^{-1}\frac{x(t)}{\left(a(t)/|a(t)|\right)R(t)} + \frac{a(t)b(t)}{|a(t)b(t)|}\varnothing(t) - m\pi \tag{51}$$

While all angle values shown in the table satisfy the unified combination-wave equation, the results demonstrate that the angle values in the colored entries adequately represent this specific spring example problem. Additionally, the angle solution changes between clockwise and counterclockwise arccosine solution types for each peak point in accordance with the spring oscillating in alignment with its combination-wave representation.

Further validation regarding multi-dimensional/multi-variable considerations are provided within the following example application of a 4D dual-cone representation of Einstein's special relativity theory.

3.3. Physics-Based Four-Dimensional Dual-Cone Application

To validate the URAM method across multi-dimensional/multi-variable considerations, it is applied within a 4D dual-cone shape representation of Einstein's special relativity theory. A spatial 3D plot of the following equation yields the dual-cone shape that expands and contracts over time, which can be viewed as a spacetime problem as shown within Figure 7 below.

$$x^2 + y^2 = \left(\sqrt{\sin(2t/\pi)}z\right)^2 \tag{52}$$

In special relativity theory, an absolute observer is located at the dual-cone's center. It is also generally possible for external observers to enter the dual-cone's space at any particular instant of time. The vibrational interaction between an external observer and a point on the dual-cone's perimeter can be modeled by the radial wave geometry of URAM theory.

Within Figure 8 below, the observer is an origin used for URAM theory application. The location of this origin varies by x_{pw} and y_{pw}. Following the dual-cone radius as it varies in terms of z and t, the URAM wave interaction is determined between the dual-cone's perimeter and the observer located by x_{pw}

and y_{pw}.

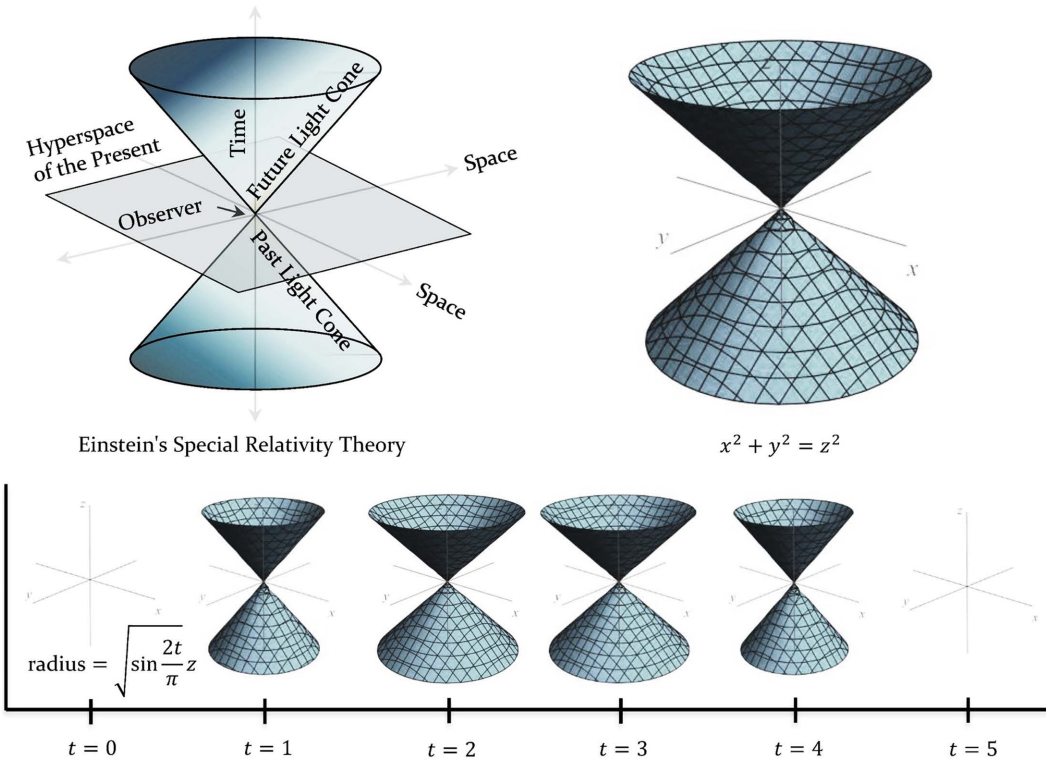

Figure 7. Einstein's special relativity theory diagram, 3D Dual-Cone Plot, and Time Evolution of the 3D Dual-Cone Plot.

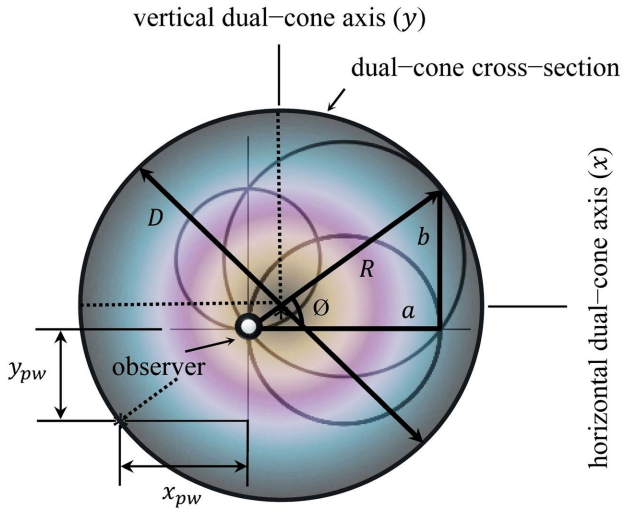

Figure 8. URAM plane wave field/frequency interaction between the observer and an edge of the dual-cone cross-section.

The dual-cone's diameter along with the observer's resultant amplitude and phase angle of vibration interaction are:

$$D(z,t) = \sqrt{\sin(2t/\pi)}|z| \tag{53}$$

$$\vec{R}\left(x_{pw}, y_{pw}, z, t\right) = D\left(z, t\right) \pm \sqrt{x_{pw}^2 + y_{pw}^2} \tag{54}$$

$$\varnothing\left(x_{pw}, y_{pw}\right) = \tan^{-1}\left|\frac{y_{pw}}{x_{pw}}\right|. \tag{55}$$

The observer's four-variable unified combination-wave equation and wave rotation solution are provided below for use when performing the numerical validation shown in Table 6 and Table 7. To note, variable c_q is determined from the parametrically driven computer-aided design sketch as shown in Figure 9 below.

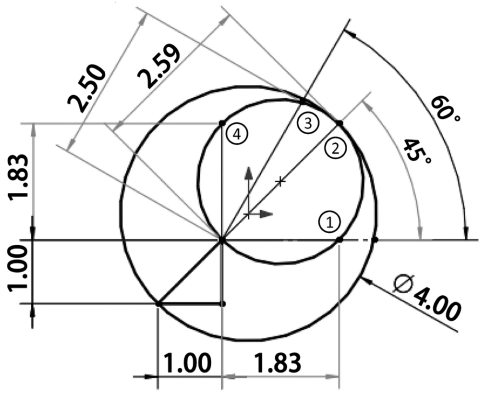

Figure 9. Computer-aided design sketch of the observer's relative angle.

Table 6. Computer-aided design data of the observer's relative angle.

Point No.	CAD Wave Numbers	CAD Wave Rotations for Each Quadrant			
#	c_q	θ_{q1}	θ_{q2}	θ_{q3}	θ_{q4}
1	1.828 427(12)	0˚	180˚	270˚	360˚
2	2.585 786(43)	45˚	135˚	225˚	315˚
3	2.497 677(89)	60˚	120˚	210˚	300˚
4	1.828 427(12)	90˚	90˚	180˚	270˚

The digits in parentheses are digits that contain potential inaccuracies.

Table 7. Computer-aided design data of the observer's relative angle.

+Spin Angles for Each Quadrant				−Spin Angles for Each Quadrant				Percent Errors-1 for Each Quadrant				Percent Errors-2 for Each Quadrant			
$\theta_{q1,1}$	$\theta_{q2,1}$	$\theta_{q3,1}$	$\theta_{q4,1}$	$\theta_{q1,2}$	$\theta_{q2,2}$	$\theta_{q3,2}$	$\theta_{q4,2}$	$E_{q1,1}$	$E_{q2,1}$	$E_{q3,1}$	$E_{q4,1}$	$E_{q1,2}$	$E_{q2,2}$	$E_{q3,2}$	$E_{q4,2}$
90.0˚	90.0˚	180.0˚	360.0˚	0.0˚	180.0˚	270.0˚	−90.0˚	N/A	N/A	N/A	0.00	0.00	0.00	0.00	N/A
45.0˚	134.9˚	224.9˚	−134.9˚	44.9˚	−224.9˚	−30.0˚	315.0˚	0.01	0.00	0.00	N/A	N/A	N/A	N/A	0.00
60.0˚	120.0˚	210.0˚	−30.0˚	30.0˚	−210.0˚	−30.0˚	299.9˚	0.00	0.00	0.00	N/A	N/A	N/A	N/A	0.00
90.0˚	90.0˚	180.0˚	0.0˚	0.0˚	−180.0˚	−90.0˚	270.0˚	0.00	0.00	0.00	N/A	N/A	N/A	N/A	0.00

The colored table entries apply to the specific example problem. The entries containing angle values that required an addition of −2π are colored in a darker color shade than the others.

$$r_C\left(\theta, x_{pw}, y_{pw}, z, t\right) = \hat{R}R\left(x_{pw}, y_{pw}, z, t\right)\cos\left(\theta + \hat{\varnothing}\varnothing\left(x_{pw}, y_{pw}\right)\right)$$
$$\Rightarrow \prod_{m=1}^{q} \mathrm{e}^{\mathrm{i}(m-1)\pi}\left(\sqrt{\sin\frac{2t}{\pi}}z \pm \sqrt{x_{pw}^2 + y_{pw}^2}\cos\left(\theta - \mathrm{e}^{\mathrm{i}(q-1)\pi}\tan\left|\frac{y_{pw}}{x_{pw}}\right|\right)\right) \tag{56}$$

$$\theta\left(x_{pw}, y_{pw}, z, t\right) = \pm\cos^{-1}\frac{c_q\left(x_{pw}, y_{pw}, z, t\right)}{\hat{R}R\left(x_{pw}, y_{pw}, z, t\right)} - \hat{\varnothing}\varnothing\left(x_{pw}, y_{pw}\right) - m\pi \tag{57}$$

The results show very small error due to the limited accuracy of the data given in Table 6. This is expected due to the use of computer-aided design. Additionally, the first point shown in Figure 9 required the clockwise angle solution type for the first three quadrants and the counterclockwise angle solution type for the fourth quadrant. The opposite of the angle solution types described for the first point(s) was required for the remaining three points extended to all four quadrants. Nevertheless, the presented simulated unified resultant amplitude methodology for multi-dimensional/multi-variable opposite wave summation is validated.

4. Conclusions

In conclusion, it was shown in the theoretical presentation that the simulated unified resultant amplitude theory unifies all four separate combination-wave equations into one equation that resolves back into their four wave fields merely from assigning the summation wave's spatial property q (or through using the absolute value operator). Moreover, the unified wave rotation solution arises from the unified combination-wave equation. This unified angle solution reduces the eight different solutions that would be derived from the four separate combination-wave equations into a single, two-component wave rotation equation. In conjunction, this unified resultant amplitude method is generalized and extended to multi-dimensional/multi-variable considerations.

In connection to a holistic systems approach, unification of the four separate combination-wave equations in addition to solving for the wave rotation solution from the unified equation enables one to perform a resultant amplitude analysis for the specified application in a unified manner rather than having to individually consider the four different possibilities for the fluctuation occurrence concerning the separate combination-wave equations. Moreover, this URAM theory can be very useful for condensing complex theories involving nested substitutions of the specific combination-wave equations. Regarding validation and the relevance of this theory, the unified resultant amplitude analysis was successfully applied within the frameworks of a simple two-dimensional kinematics example, a generalized spring system, and a four-dimensional dual-cone problem in relation to the generalized unified wave equation and wave rotation solution.

5. Future Research

Future extension of this research involves the application toward generalization of a complex theoretical development of a self-centering cam which substantiates

the practical engineering usefulness of the unified resultant amplitude theory presented herein. Furthermore, we foresee that an extension of the unified resultant amplitude theory for opposite wave summation may lead to Fourier series unification for providing a more holistic approach that may be useful for applications involving this series.

From a mathematical view, the unified wave equation discloses interesting effects occurring at the fundamental mathematical level due to its simplicity and elimination of separation through the connection of all four quadrants. In relation to such, there are indications that the unified resultant amplitude theory may have a variety of important implications regarding unified field theory in connection with Schrödinger's 3D particle wave equation and recently emerging quantum gravity techniques [21]-[25]. Moreover, future potential research regarding the development of a unified field theory involving unification of the four fundamental forces on the conceivable basis of quantum gravity embedded with Haramein's description of a wave-based/holographic structure of spacetime may commence.

In conjunction, through related prospective research endeavors, we may show that geometries arising from the unified combination-wave are associated with the three-dimensional manifold of spacetime in Haramein's efforts to amend Einstein's field equations and solve for a modified Kerr-Newman metric for an inclusion of torque and Coriolis forces within the framework of U_4 space for describing the origin of spin [13]. Additionally, circular constructions from the unified resultant wave may have a related association with an information wormhole network for describing the nexus of energy entanglement related to spacetime [23] [24]. In connection with the geometrical properties of this unified amplitude theory, as Wheeler mentions, "*The vision of quantum gravity is a vision of turbulence—turbulent space, turbulent time, turbulent spacetime…spacetime in small enough regions should not be merely 'bumpy', not merely erratic in its curvature, it should fractionate into ever-changing, multiply-connected geometries*" [25].

Acknowledgements

The author would like to acknowledge the efforts undergone by Dr. Terrence L. Chambers, Donald & Janice Mosing BORSF Endowed Chair in Mechanical Engineering at the University of Louisiana at Lafayette, and thank him for providing supervision, writing review, and constructive feedback which helped improved this research.

Conflicts of Interest

The author has no conflicts of interest with this work.

References

[1] Tse, F.S., Morse, I.E. and Hinkle, R.T. (1978) Mechanical Vibrations—Theory and Application. 2nd Edition, Allyn and Bacon.

[2] Shigley, J. and Uicker, J. (1995) Theory of Machines and Mechanisms. 2nd Edition,

McGraw Hill.

[3] Diprima, B. (1996) Elementary Differential Equations and Boundary Value Problems. 6th Edition, John Wiley & Sons.

[4] Hughes-Hallett, D., Gleadon, A.M., *et al.* (1994) Calculus. John Wiley & Sons.

[5] Appendix 2 Waves and Wave Analysis.

[6] Hibbler, R.C. (1974) Engineering Mechanics Dynamics, 7th Edition, Prentice Hall.

[7] Lienhard IV, J.H. and Lienhard V, J.H. (2019) A Heat Transfer Textbook. 5th Edition, Dover Publications.

[8] Roberson, J.A. and Crowe, C.T. (1980) Engineering Fluid Mechanics. 2nd Edition, Washington State University, Houghton Mifflin Company.

[9] Liu, S., Cao, S., Han, Z., Liu, J., Li, S. and Xu, Z. (2023) Modeling the Flow Deflection Characteristics of Incompressible Fluids in the Vortex Chamber and Analysis of Its Influencing Parameters. https://doi.org/10.21203/rs.3.rs-3022713/v1

[10] Moore, J.T. (2011) Chemistry for Dummies. 2nd Edition, Wiley Publishing.

[11] Lehrman, R.L. (2009) E-Z Physics. 4th Edition, Barron's Educational Series, Inc.

[12] Dymnikov, A.D. (2013) The Matrix Theory of Mathematical Field and the Motion of Mathematical Points in N-Dimensional Metric Space. *Journal of Computational Methods in Sciences and Engineering*, **13**, 59-109. https://doi.org/10.3233/jcm-120454

[13] Haramein, N. and Rauscher, E.A. (2005) The Origin of Spin: A Consideration of Torque and Coriolis Forces in Einstein's Field Equations and Grand Unification Theory. In: Amoroso, R.L., Lehnrt, B. and Vigier, J.P., Eds., *Beyond the Standard Model: Searching for Unity in Physics*, The Noetic Press, 153-168.

[14] Engin, D., Cross, M.C. and Yariv, A. (1997) Amplitude-Equation Formalism for Four-Wave-Mixing Geometry with Transmission Gratings. *Journal of the Optical Society of America B*, **14**, 3349-3361. https://doi.org/10.1364/josab.14.003349

[15] Cuyt, A. and Lee, W. (2023) Multiscale matrix pencils for separable reconstruction problems. *Numerical Algorithms*, **95**, 31-72. https://doi.org/10.1007/s11075-023-01564-3

[16] Webb, G.M., Hu, Q., Dasgupta, B., Roberts, D.A. and Zank, G.P. (2010) Alfvén Simple Waves: Euler Potentials and Magnetic Helicity. *The Astrophysical Journal*, **725**, 2128-2151. https://doi.org/10.1088/0004-637x/725/2/2128

[17] Islam, S.M.R., Kumar, D. and Akbar, M.A. (2021) Unified Method Applied to the New Hamiltonian Amplitude Equation: Wave Solutions and Stability Analysis. https://doi.org/10.21203/rs.3.rs-1087623/v1

[18] Baldwin, J.T. (2014) The Complex Numbers and Complex Exponentiation: Why Infinitary Logic Is Necessary. *Lecturas Matematicas*, No. 2006, 117-135.

[19] Prots'ko, I. and Gryshchuk, O. (2022) The Modular Exponentiation with Precomputation of Redused Set of Residues for Fixed-Base. *Radio Electronics, Computer Science, Control*, No. 1, 58. https://doi.org/10.15588/1607-3274-2022-1-7

[20] Köplinger, J. and Shuster, J.A. (2023) Exceptional Infinite Fields with Distributive Exponentiation. https://www.researchgate.net/profile/Jens-Koeplinger/publication/368898811_Exceptional_finite_fields_with_distributive_exponentiation/links/6447b935017bc07902dae36a/Exceptional-finite-fields-with-distributive-exponentiation.pdf

[21] Haramein, N. (2013) Quantum Gravity and Holographic Mass. *Physical Review and*

Research International, **3**, 270-292.

[22] Haramein, N., Guermonprez, C. and Alirol, O. (2024) The Origin of Mass and the Nature of Gravity. International Space Federation Laboratory, 1-52.

[23] Haramein, N., Brown, W.D. and Val Baker, A. (2016) The Unified Spacememory Network: From Cosmogenesis to Consciousness. *NeuroQuantology*, **14**, 1-15. https://doi.org/10.14704/nq.2016.14.4.961

[24] Brown, W. (2019) Unified Physics and the Entanglement Nexus of Awareness. *NeuroQuantology*, **17**, 40-52. https://doi.org/10.14704/nq.2019.17.7.2519

[25] Ford, K.W. and Wheeler, J.A. (1998) Geons, Black Holes and Quantum Foam—A Life in Physics. W. W. Norton and Co.